Journal of King Saud University – Computer and Information Sciences (2017) 29, 39–53

King Saud University

Journal of King Saud University – Computer and Information Sciences

www.ksu.edu.sa
www.sciencedirect.com

Blind separation of multicomponent seismic wavefield using SVD of reduced dimension spectral matrix

Abdullah Al-Hasanat [a], Abdelwadood Mesleh [b,*], Monther Krishan [c], Ahmed Sharadqh [b], Aws Al-Qaisi [d], W.L. Woo [e], S.S. Dlay [e]

[a] *Dept. of Computer Engineering, Faculty of Engineering, University of Al-Hussien Bin Talal, Jordan*
[b] *Computer Engineering Dept., Faculty of Engineering Technology, Al-Balqa' Applied University, Jordan*
[c] *Mechatronics Engineering Dept., Faculty of Engineering Technology, Al-Balqa' Applied University, Jordan*
[d] *Communication Engineering Dept., Faculty of Engineering Technology, Al-Balqa' Applied University, Jordan*
[e] *School of Electrical, Electronic & Computer Engineering, Newcastle University, England*

Received 10 August 2015; revised 20 January 2016; accepted 25 January 2016
Available online 28 March 2016

KEYWORDS

Blind separation;
Multicomponent seismic wavefield;
SVD

Abstract This paper presents a blind separation algorithm based on singular value decomposition (SVD) of reduced dimension spectral matrix. Furthermore, a mathematical matrix model of the multicomponent seismic wavefield is developed as a framework for implementing the proposed algorithm. The proposed blind separation algorithm organizes the frequency transformed multicomponent seismic wavefield into one long data vector. The blind separation of the desired seismic wavefield is accomplished by projecting the long data vector onto the eigenvectors of the dimensionally reduced spectral matrix according to the energy of the eigenvalues. The proposed algorithm is tested on both synthetic and real multicomponent seismic wavefields. Results show outstanding performance compared to the MC-WBSMF algorithm. Therefore, the computational complexity is reduced by a factor greater than 14,400 and there is an improvement in accuracy of 17.5%.

1. Introduction

In seismic exploration, a wavelet is sent to the earth layers and the reflected seismic wavefields, due to the impedance mismatches between different geological layers, are recorded by linear arrays of multi-component sensors (Al-Qaisi et al., 2008). The recorded geophysical data are often contaminated by multiple interference, first arrivals and random noise. The main objective of seismic data processing is to identify and

* Corresponding author.
Peer review under responsibility of King Saud University.

Production and hosting by Elsevier

http://dx.doi.org/10.1016/j.jksuci.2016.01.006

separate different seismic waves to obtain a better interpretation of the seismic wavefield data (Al-Qaisi et al., 2008; Hanna, 1988). In single component sensor arrays, many conventional techniques have been developed but they all have their drawbacks. Radon transform can be used to enhance reflection events in a seismic wavefields. However, this technique has poor performance in the case of short arrays (Foster and Mosher, 1992). F-K transform technique decomposes the seismic wavefield data into the frequency–wave number domain where the plane waves can be identified. Nevertheless, the use of this transform puts limitations on the types of data that can be examined. For example, it has a poor performance in the presence of non-plane waves (Embree et al., 1963; Zhou and Greenhalgh, 2006). The method of τ–p transform characterizes a point source shot record as a sequence of plane wave tests, so it is closely linked to the F-K transform in the sense that the τ–p technique can be considered as a time-variant F-K technique. As a result, both techniques experience similar restrictions (Al-anboori et al., 2005; Benoliel and Schneider, 2006). In recent times, multicomponent sensors array technology has witnessed tremendous growth in seismic exploration. Principally, separation techniques are needed for a noisy multicomponent seismic wavefield. The basic SVD approaches which were previously developed for single component sensor arrays have been extended to handle data collected from multicomponent sensor arrays. For example, the SVD of quaternion matrices and SVD compound with partial independent component analysis (ICA) are capable of separating and identifying different seismic waves (Le Bihan and Mars, 2004; Vrabie et al., 2004). Yet, these techniques require a pre-processing step for wave alignment. Filtering and seismic wavefield separation can be performed in the frequency domain and is called spectral-matrix filtering (Rutty and Jackson, 1992; Mari and Glangeaud, 1990). However, it is computationally expensive to diagonalize the whole spectral matrix. To alleviate these problems, the proposed algorithm which is derived from MC-WBSMF algorithm (Paulus and Jerome and Mars, 2006; Paulus et al., 2005) reduces the dimensions of the estimated multicomponent spectral covariance matrix and combines the SVD technique under unique mathematical identifiability conditions. In (Liu, 2014), Liu proposed a separation method of P- and SV-waves based on polarization rotation, in which adaptive sliding windows are used and adopted in the separation of wavefields of crosswell seismic data. However, considering the time dependence of seismic signals, Liu determined the width of the time windows automatically in a time varying polarization analysis. In our method, the separation of seismic waves based on the difference between eigenvalues of the reduced dimensional spectral covariance matrix eigenvectors. In Ling and Ren (2013), an independent component analysis-based principal component regression is adopted for BSS problem.

In this paper, we propose a blind algorithm based on SVD of reduced dimension multicomponent spectral covariance matrix to separate different seismic waves from a noisy multicomponent seismic wavefield. The eigenvector matrix of spectral matrix has been estimated by means of the eigenvector matrix of reduced dimension spectral matrix using SVD. This spectral covariance matrix with reduced dimension has been constructed from creating a matrix that contains concatenated versions of long data vectors. This long data vector has been created by reorganizing the frequency transform of recorded multicomponent seismic wavefield data into one column vector. In the proposed separation algorithm, the seismic wavefield data subspaces are defined by the eigenvector matrix which is derived from the SVD of reduced dimension spectral matrix. Furthermore, the blind separation of the required seismic wavefield is accomplished by projecting the long data vector onto the eigenvectors of the spectral matrix according to the energy of the eigenvalues. The contribution of this work can be stated as follows: Firstly, a frequency transformed matrix model of a noisy multicomponent seismic wavefield has been proposed. Secondly, a computational efficient algorithm that significantly reduces the spectral covariance matrix dimensions has been mathematically and analytically implemented.

The paper has been organized as follows: Section 2 develops and derives the time domain noisy multicomponent seismic wavefield model in the form of frequency transformed matrix model. Section 3 illustrates the mathematical analysis of the proposed technique by addressing the reduction of spectral covariance matrix dimension, deriving the eigenvector matrix of spectral matrix from the eigenvector matrix of the reduced dimension spectral matrix and separating different seismic waves from a noisy multicomponent seismic wavefield. Section 4 discusses the performance of the proposed algorithm on real noisy multicomponent seismic wavefield. Finally, Section 5 concludes the paper.

2. The proposed mathematical model for multicomponent seismic wavefield

In this section, the proposed mathematical model for multicomponent seismic wavefield is presented. Consider a uniform linear array as shown in Fig. 1 that consists of K_x multicomponent sensors recording the propagation of seismic waves as well as ground roll with $P < K_x$ where P represents the number of seismic waves. The multi-component seismic wavefield data that are recorded during K_t samples on the dth component ($d = 1,\ldots,K_d$) of the ith sensor ($i = 1,\ldots,K_x$) with additive noise can be expressed mathematically as in Eq. (1):

$$y_{i,d}(t) = \sum_{p=1}^{P} \alpha_{d,p} e^{j\varphi_{d,p}} a_{d,p} w_p(t - \tau_{i,d}(\theta_p)) + b_{i,d}(t) \tag{1}$$

where $\alpha_{d,p}$ is the attenuation factor, the parameters $\varphi_{d,p}$ represent the phase changing between different components, the parameter $\alpha_{d,p}$ is the amplitude of the pth seismic wave, $w_p(t)$ is the emitted seismic wavelet, the parameter $\tau_{i,d}(\theta_p)$ is the time delay observed at the ith sensor with direction of arrival θ_p, and $b_{i,d}(t)$ is the white Gaussian noise, which is uncorrelated with the seismic waves.

From Eq. (1), it follows that the multicomponent seismic data sets shown in Fig. 2 can be represented as in Eq. (2):

$$\underset{\equiv}{Y_T} \in \mathsf{E}^{K_d \times K_x \times K_t} \tag{2}$$

where K_d, K_x and K_t represent the number of sensor components, the number of sensors and the recorded samples for each seismic trace, respectively. By applying the Fourier Transform to Eq. (1), the multi-component seismic model can be represented as a set of instantaneous mixture of traces as given in Eq. (3):

$$\underset{\equiv}{Y} = FT\{\underset{\equiv}{Y_T}\} \in \mathsf{d}^{K_d \times K_x \times K_f} \tag{3}$$

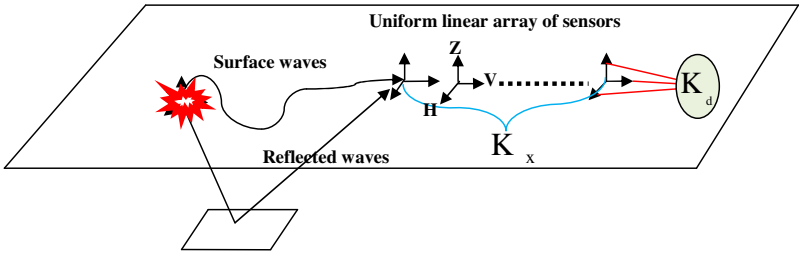

Figure 1 Recording the seismic wavefield using a linear multicomponent geophones array.

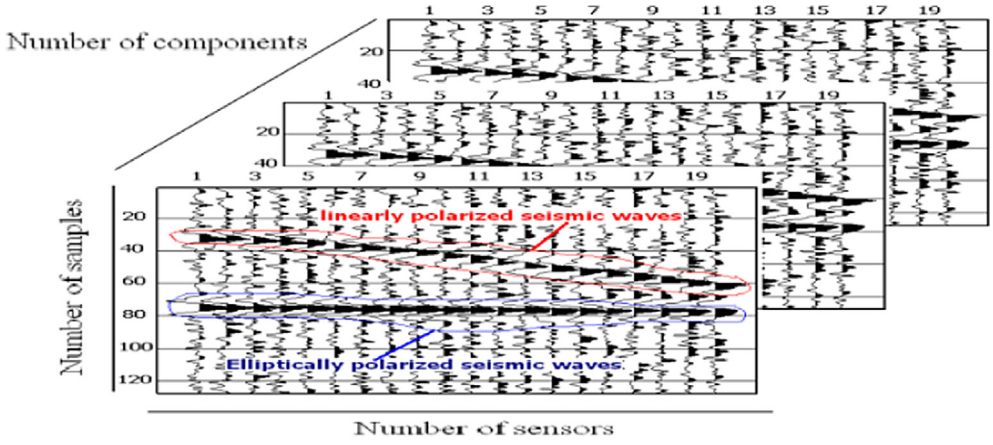

Figure 2 Multi-component wavefield seismic data set.

where K_f is number of frequency bins. The available information in Eq. (3) can be rearranged into a long data vector as shown in Eq. (4) (Hendrick, 2006):

$$\mathbf{y}(f) = [\mathbf{h}(f_1)^T \ldots \mathbf{h}(f_{K_f})^T, \mathbf{v}(f_1)^T \ldots \mathbf{v}(f_{K_f})^T, \mathbf{z}(f_1)^T \ldots \mathbf{z}(f_{K_f})^T]^T \tag{4}$$

where $\mathbf{h}(f_{K_f}), \mathbf{v}(f_{K_f}), \mathbf{z}(f_{K_f})$ are vectors of size (K_x) related to the fth frequency bin of the seismic waves received on K_x sensors.

The long data vector $\mathbf{y}(f)$ that is shown in Fig. 3 can be expressed in matrix form as in Eq. (5):

$$\underbrace{\mathbf{y}(f)}_{(m\times 1)} = \underbrace{\mathbf{X}(f)}_{(m\times P)} \underbrace{\mathbf{a}}_{(P\times 1)} + \underbrace{\mathbf{b}(f)}_{(m\times 1)} \tag{5}$$

where,

(i) $\mathbf{a} = [a_1, a_2, \ldots, a_p]^T$ corresponds to the random wave amplitude of size $(P \times 1)$.

(ii) $\mathbf{b}(f)$ is the noise vector of size $((m = K_d K_x K_f) \times 1)$.

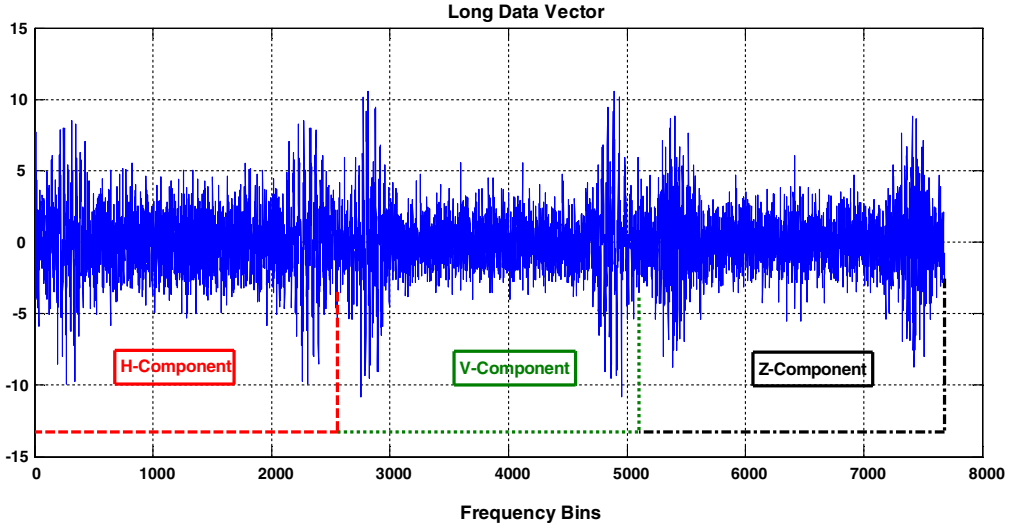

Figure 3 The real part of the long data vector $\mathbf{y}(f)$ that contains all the frequency bins on all sensors for each component.

(iii) $\mathbf{X}(f) = [\mathbf{x}_1(f), \ldots\ldots, \mathbf{x}_p(f), \ldots\ldots \mathbf{x}_P(f)]$ is a matrix of size $((m = K_d K_x K_f) \times P)$ with $p = 1, \cdots, P$ with

$$\mathbf{x}_p(f) = \begin{bmatrix} \underline{x}_p(f) \\ \alpha_p e^{j\varphi_p} \underline{x}_p(f) \\ \beta_p e^{j\psi_p} \underline{x}_p(f) \end{bmatrix} = \begin{bmatrix} c1 \\ \alpha_p e^{j\varphi_p} \\ \beta_p e^{j\psi_p} \end{bmatrix} \otimes \underline{x}_p(f) \tag{6}$$

and '$\otimes$' is the Kronecker product. The column vector $\underline{x}_p(f)$ expressed as in Eq. (7):

$$\underline{x}_p(f) = \begin{bmatrix} l_{p,f_{f_1}} \\ l_{p,f_{f_2}} \\ \vdots \\ l_{p,f_{K_f}} \end{bmatrix} = \begin{bmatrix} w_p(f_1)\mathbf{c}(\theta_p, f_1) \\ w_p(f_2)\mathbf{c}(\theta_p, f_2) \\ \vdots \\ w_p(f_{K_F})\mathbf{c}(\theta_p, f_{K_f}) \end{bmatrix}$$

$$= \overbrace{\begin{bmatrix} \mathbf{c}(\theta_p, f_1) & 0 & \ldots & 0 \\ 0 & \mathbf{c}(\theta_p, f_2) & & \vdots \\ \vdots & & \ddots & 0 \\ 0 & \ldots & 0 & \mathbf{c}(\theta_p, f_{K_f}) \end{bmatrix}}^{\mathbf{C}(\theta_p, f_{K_f})} \mathbf{w}_p(f) \tag{7}$$

$$\text{where } \mathbf{c}(\theta_p, f_{K_f}) = \begin{pmatrix} e^{j2\pi f_{K_f} \tau_1(\theta_p)} \\ \vdots \\ e^{j2\pi f_{K_f} \tau_i(\theta_p)} \\ \vdots \\ e^{j2\pi f_{K_f} \tau_{K_x}(\theta_p)} \end{pmatrix}$$

Finally, the $X_p(f)$ vector can be represented using the Kronecker product as in Eq. (8):

$$\mathbf{x}_p(f) = \begin{bmatrix} 1 \\ \alpha_p e^{j\varphi_p} \\ \beta_p e^{j\psi_p} \end{bmatrix} \otimes \mathbf{C}(\theta_p, f_{K_f}) \mathbf{w}_p(f)$$

$$= \overbrace{\left(\begin{bmatrix} 1 \\ \alpha_p e^{j\varphi_p} \\ \beta_p e^{j\psi_p} \end{bmatrix} \otimes \mathbf{C}(\theta_p, f_{K_f}) \right)}^{Q(\alpha_p, \beta_p, \psi_p, \theta_p, \varphi_p, f_{K_f}, \tau_{K_x})} \underbrace{\begin{matrix} \mathbf{w}_p(f) \\ wavelet \\ (1 \otimes \mathbf{w}_p(f)) \end{matrix}}$$

$$= Q(\alpha_p, \beta_p, \psi_p, \theta_p, \varphi_p, f_{K_f}, \tau_{K_x}) \mathbf{w}_p(f) \tag{8}$$

From the above equations, the matrix $X(f)$ contains the information about the seismic waves and is characterized by:

i. The direction of arrival of the seismic source θ_p.
ii. The offset τ_{K_x} that corresponds to the time of propagation between the source and the reference sensor.
iii. The attenuation factors α_p, β_p.
iv. The parameters φ_p, ψ_p describe the change of phases between H, V, and Z components.
v. The emitted seismic wavelet $w_p(f)$.
vi. The propagation characteristic term $Q(\alpha_p, \beta_p, \psi_p, \theta_p, \varphi_p, f_{K_f}, \tau_{K_x})$ that describes the multicomponent array response of the received waves.

From above, the time domain multicomponent seismic wavefield model in Eq. (1) has been transformed into frequency domain matrix model. This matrix model has been expressed by the long vector $\mathbf{y}(f)$ that contains all the frequency bins on all sensors for each component.

3. The proposed blind seismic wavefield separation algorithm

In this section, the proposed blind separation algorithm will be mathematically derived. This blind algorithm separates different seismic waves according to their energy. $\mathbf{E}_{yy}(f)$ is a $m \times m$ matrix as shown in Eq. (9), where $m = K_d K_x K_f$. Therefore, the presented multicomponent covariance spectral matrix is composed of $(K_d K_f)^2$ blocks of dimension $K_x K_x$. Every block characterizes the correlation between the various directional components of the received waves on all sensors at different frequencies. Hence, the structure of the covariance matrix is expressed in Eq. (9) (Paulus and Jerome and Mars, 2006; Kirlin, 2001):

$$\mathbf{E}_{\mathbf{yy}}(f) = \begin{pmatrix} \mathbf{E}_{H,H}(f) & \mathbf{E}_{H,V}(f) & \mathbf{E}_{H,Z}(f) \\ \mathbf{E}_{V,H}(f) & \mathbf{E}_{V,V}(f) & \mathbf{E}_{V,Z}(f) \\ \mathbf{E}_{Z,H}(f) & \mathbf{E}_{Z,V}(f) & \mathbf{E}_{Z,Z}(f) \end{pmatrix} \tag{9}$$

The component blocks $\mathbf{E}_{H,H}(f)$, $\mathbf{E}_{V,V}(f)$, $\mathbf{E}_{Z,Z}(f)$ are placed on the main diagonal of the covariance spectral matrix. As the received seismic waves on the components H, V, Z are correlated, the cross-component blocks hold information regarding the interaction between the various components, as well as the polarization. A jointly spatial and frequency smoothing operator can be applied to perform an estimation of noninvertible unity rank spectral covariance matrix (Eq. (10)) (Rao and Hari, 1993; Pillai and Kwon, 1989).

$$\hat{\mathbf{E}}_{\mathbf{yy}}(f) = \frac{1}{N} \sum_{n_s=1}^{2N_s+1} \sum_{n_f=1}^{2N_f+1} \mathbf{y}_{n_s,n_f}(f) \mathbf{y}_{n_s,n_f}^H(f) \tag{10}$$

where $N = (2N_S + 1)(2N_f + 1)$, noting that the vector $\mathbf{y}_{n_s,n_f}(f)$ corresponds to a concatenation of seismic waves received on the n_s^{th} sub array and n_f^{th} sub band respectively. Fig. 4 shows a diagram of a very large estimated spectral covariance matrix $\hat{\mathbf{E}}_{\mathbf{yy}}(f)$ with dimension $(m \times m)$, the dark and light areas show signal strengths. The white areas indicate where the signal strength is high and the dark areas are where there is no signal. Furthermore, it can be noticed that it is extremely computationally expensive to diagonalize the whole estimated spectral covariance matrix.

For this reason, a new matrix $\mathbf{R}(f)$ of size $(m \times N)$ that contains concatenated long-vectors resultant from the spatial and frequency smoothing can be proposed as in Eq. (11) (Paulus et al., 2005; Pillai and Kwon, 1989).

$$\mathbf{R}(f) = \overbrace{\begin{bmatrix} \vdots & \vdots & \vdots & \vdots \\ \mathbf{y}_{1,1}(f) & \cdots \; \mathbf{y}_{2N_s+1,1}(f) & \cdots \; \mathbf{y}_{1,2N_f+1}(f) & \cdots \; \mathbf{y}_{2N_s+1,2N_f+1}(f) \\ \vdots & \vdots & \vdots & \vdots \end{bmatrix}}^{N=(2N_S+1)(2N_F+1)} \tag{11}$$

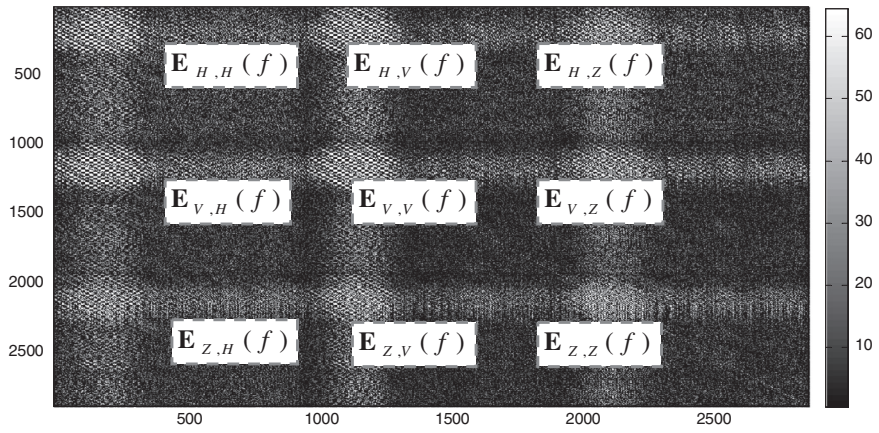

Figure 4 Multicomponent spectral covariance matrix.

The estimated spectral covariance matrix can be mathematically written as in Eq. (12):

$$\hat{\mathbf{E}}_{\mathbf{yy}1}(f) = \frac{1}{N}\mathbf{R}(f)\mathbf{R}^H(f) \tag{12}$$

In an alternative implementation, we will later use Eq. (13) instead of Eq. (12):

$$\hat{\mathbf{E}}_{\mathbf{yy}2}(f) = \frac{1}{N}\mathbf{R}^H(f)\mathbf{R}(f) \tag{13}$$

The frequency SVD of matrix $\boldsymbol{R}$ is given as in Eq. (14):

$$\mathbf{R}(f) = \mathbf{U}(f)\mathbf{\Lambda}(f)\mathbf{V}^H(f) = \mathbf{U}(f)\begin{bmatrix} \sqrt{\delta_1} & 0 & 0 \\ 0 & \ddots & 0 \\ 0 & 0 & \sqrt{\delta_N} \\ & & \\ 0 & \cdots & 0 \\ \vdots & & \vdots \\ 0 & \cdots & 0 \end{bmatrix}\mathbf{V}^H(f) \tag{14}$$

where $\mathbf{\Lambda}(f)$ is a diagonal matrix that holds the singular values of matrix $\mathbf{R}(f)$ noted as $\sqrt{\delta_N}$. Whereas $\mathbf{U}(f)$ and $V^H(f)$ are the orthogonal matrices that contain the left and right singular vectors in their columns. The computation of spectral matrix in Eq. (12) using SVD can be written as in Eq. (15):

$$\hat{\mathbf{E}}_{\mathbf{yy}1}(f) = \frac{1}{N}\mathbf{R}(f)\mathbf{R}^H(f) = \frac{1}{N}(\mathbf{U}(f)\mathbf{\Lambda}(f)\mathbf{\Lambda}^H(f)\mathbf{U}^H(f)) = \frac{1}{N}\left[\mathbf{U}(f)\left[\begin{bmatrix} \delta_1 & & \\ & \ddots & \\ & & \delta_N \end{bmatrix}\begin{matrix} 0 \\ \\ \\ 0 \end{matrix}\right]\mathbf{U}^H(f)\right] \tag{15}$$

It is very important to identify the eigenvector matrix $\mathbf{U}(f)$. However, it is computationally expensive to decompose the spectral matrix $\hat{\mathbf{E}}_{\mathbf{yy}1}(f)$. Therefore, it is time consuming to compute the eigenvector matrix according to Eq. (15). To solve this, a considerable reduction of the estimated spectral matrix dimension can be obtained if the formation of the spectral matrix is mathematically derived using SVD as in Eq. (16):

$$\begin{aligned}\hat{\mathbf{E}}_{\mathbf{yy}2}(f) &= \frac{1}{N}\mathbf{R}^H(f)\mathbf{R}(f) == \frac{1}{N}(\mathbf{V}(f)\mathbf{\Lambda}^H(f)\Lambda(f)\mathbf{V}^H(f)) \\ &= \frac{1}{N}\left[\mathbf{V}(f)\begin{bmatrix} \delta_1 & & 0 \\ & \ddots & \\ 0 & & \delta_N \end{bmatrix}\mathbf{V}^H(f)\right]\end{aligned} \tag{16}$$

From the above, the most interesting finding is that the eigenvector matrix $\mathbf{U}(f)$ of the spectral covariance matrix in Eq. (16) can be related to the eigenvector matrix $\mathbf{V}(f)$ of reduced dimension spectral covariance matrix $\hat{\mathbf{E}}_{\mathbf{yy}2}(f)$ as in Eq. (17):

$$\mathbf{U}(f) = \mathbf{R}(f)\mathbf{V}^H(f) = \begin{bmatrix} \sqrt{\delta_1} & 0 & \cdots & 0 \\ 0 & \ddots & \ddots & \vdots \\ \vdots & \ddots & \ddots & 0 \\ 0 & \cdots & 0 & \sqrt{\delta_N} \end{bmatrix} \tag{17}$$

In other words, the eigenvector matrix $\mathbf{U}(f)$ of spectral matrix $\hat{\mathbf{E}}_{\mathbf{yy}1}(f)$ has been obtained through the eigenvector matrix $\mathbf{V}(f)$ of reduced dimension spectral matrix $\hat{\mathbf{E}}_{\mathbf{yy}2}(f)$ that is shown in Fig. 5.

As a result, the size of eigenvector matrix $\mathbf{U}(f)$ has been reduced from $(m \times m)$ to $(N \times N)$ where $(N \ll m)$, for example, in Fig. 4, the spectral matrix has $m = 3000$, on the other hand, in Fig. 5, the reduced dimension of the spectral matrix has $N = 25$. Hence, the complexity is reduced by a factor greater

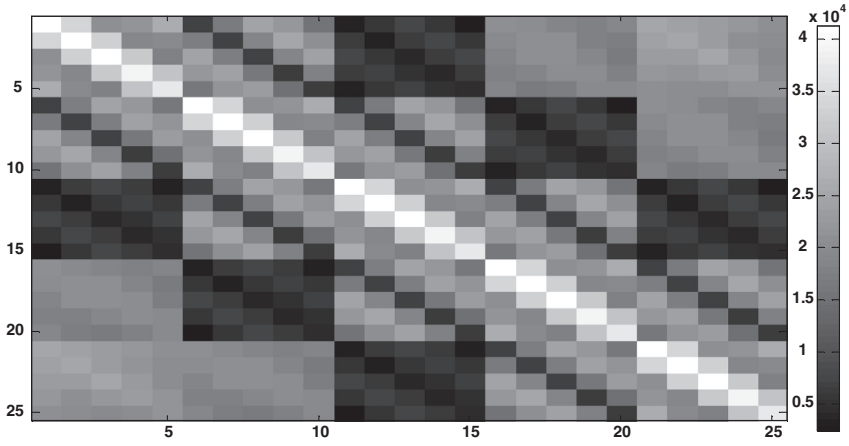

Figure 5 Reduced dimension covariance spectral matrix.

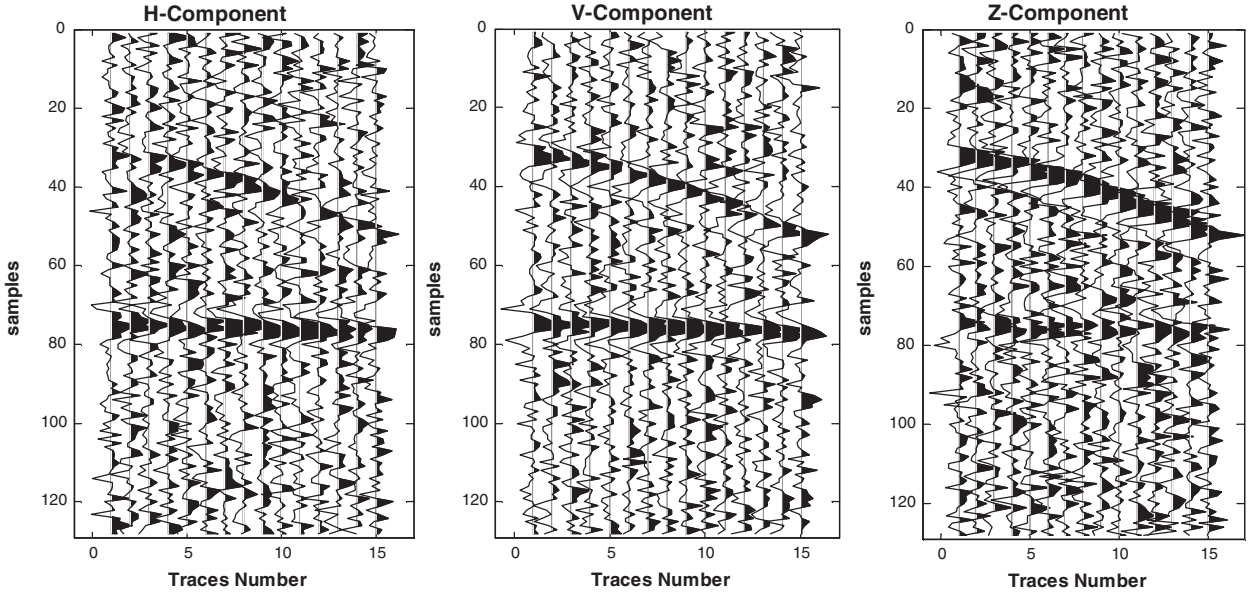

Figure 6 Noisy seismic wavefield data set that are recorded on linear array of three component sensors.

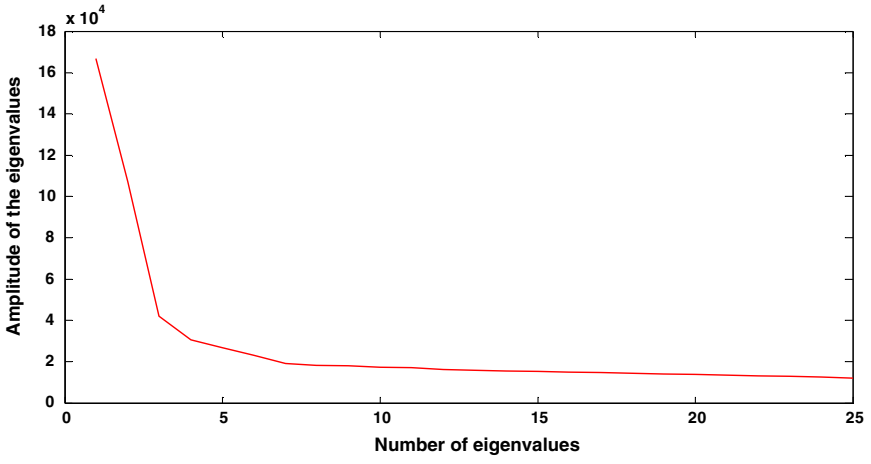

Figure 7 Eigenvalues of estimated reduced dimension covariance spectral matrix.

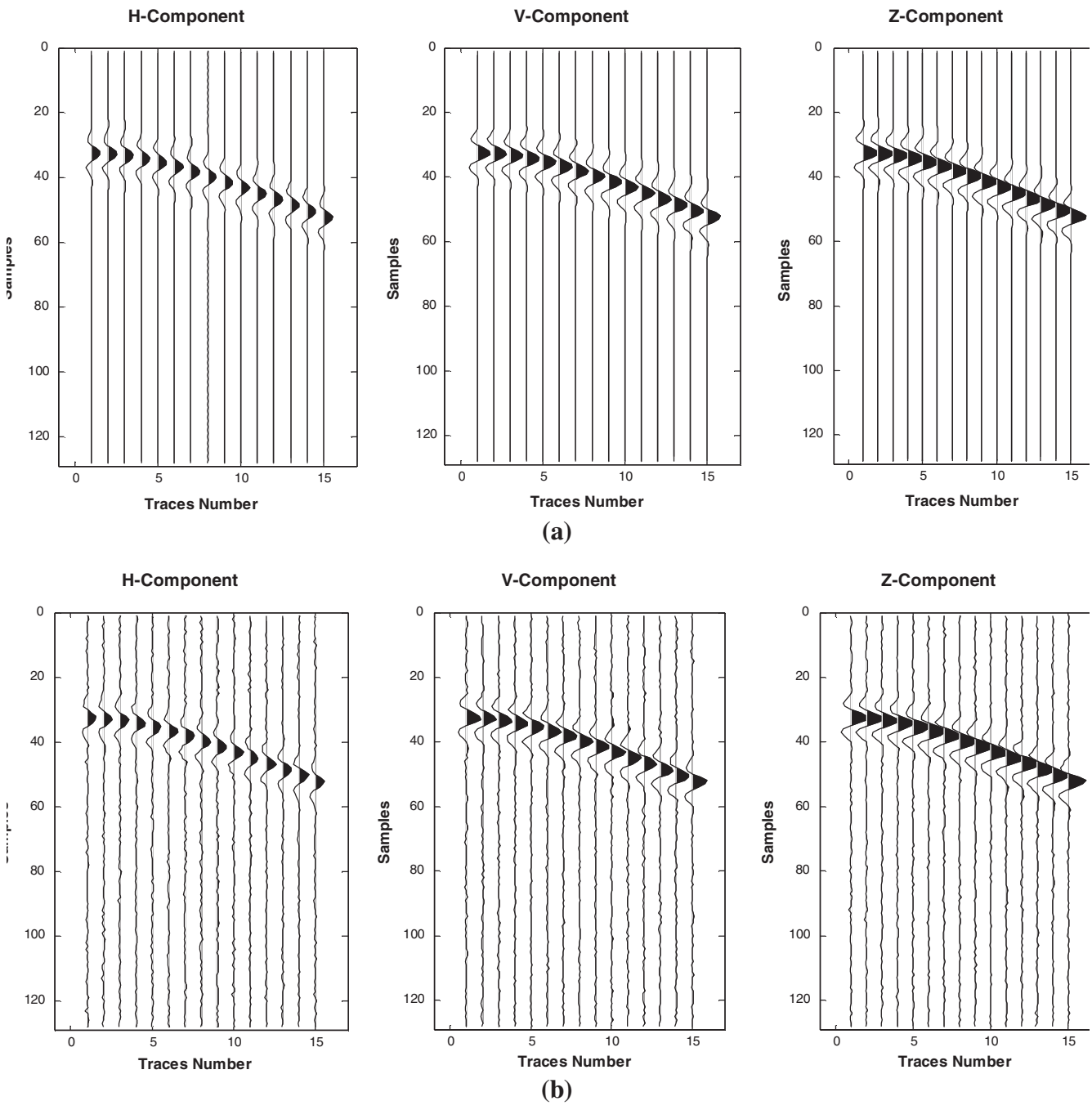

Figure 8 (a) Multicomponent seismic wavefield model for first wave. (b) First separated seismic wave from noisy multicomponent seismic wavefield data set.

than 14,400. Therefore, the reduced dimension eigenvector matrix $\mathbf{U}(f)$ in Eq. (17) is highly important as it has significant implications for developing a less complex algorithm. The following steps will show the ability of the proposed algorithm to separate different seismic waves according to their energy. The $\hat{\mathbf{E}}_{\mathbf{yy}1}(f)$ matrix is expressed in Eq. (18):

$$\begin{aligned}\hat{\mathbf{E}}_{\mathbf{yy}1}(f) &= \hat{\mathbf{E}}_{\mathbf{Xa},wave1}(f) + \hat{\mathbf{E}}_{\mathbf{Xa},wave2}(f) + \hat{\mathbf{E}}_{\mathbf{bb}} \\ &= \lambda_1 \mathbf{u}_1(f)\mathbf{u}_1^H(f) + \lambda_2 \mathbf{u}_2(f)\mathbf{u}_2^H(f) + \sigma_b^2 \mathbf{I}(f) \end{aligned} \tag{18}$$

where $\hat{\mathbf{E}}_{\mathbf{Xa},wave1}(f) = \lambda_1 \mathbf{u}_1(f)\mathbf{u}_1^H(f)$ and $\hat{\mathbf{E}}_{\mathbf{Xa},wave2}(f) = \lambda_2 \mathbf{u}_2(f)\mathbf{u}_2^H(f)$, noting that the vector $\mathbf{u}_1(f)$ is the first eigenvector that corresponds to the first highest eigenvalue λ_1, the vector $\mathbf{u}_2(f)$ is the second eigenvector that corresponds to the second highest eigenvalue λ_2 and $\hat{\mathbf{E}}_{\mathbf{bb}}(f) = \sigma_b^2 \mathbf{I}$ represents the noise subspace of the noise vector $\mathbf{b}(f)$. The eigenvector matrix $\mathbf{U}(f)$ completely specifies the column vectors in $\mathbf{X}(f)$ matrix up to scale factors if and only if the seismic waves have a distinct spectral

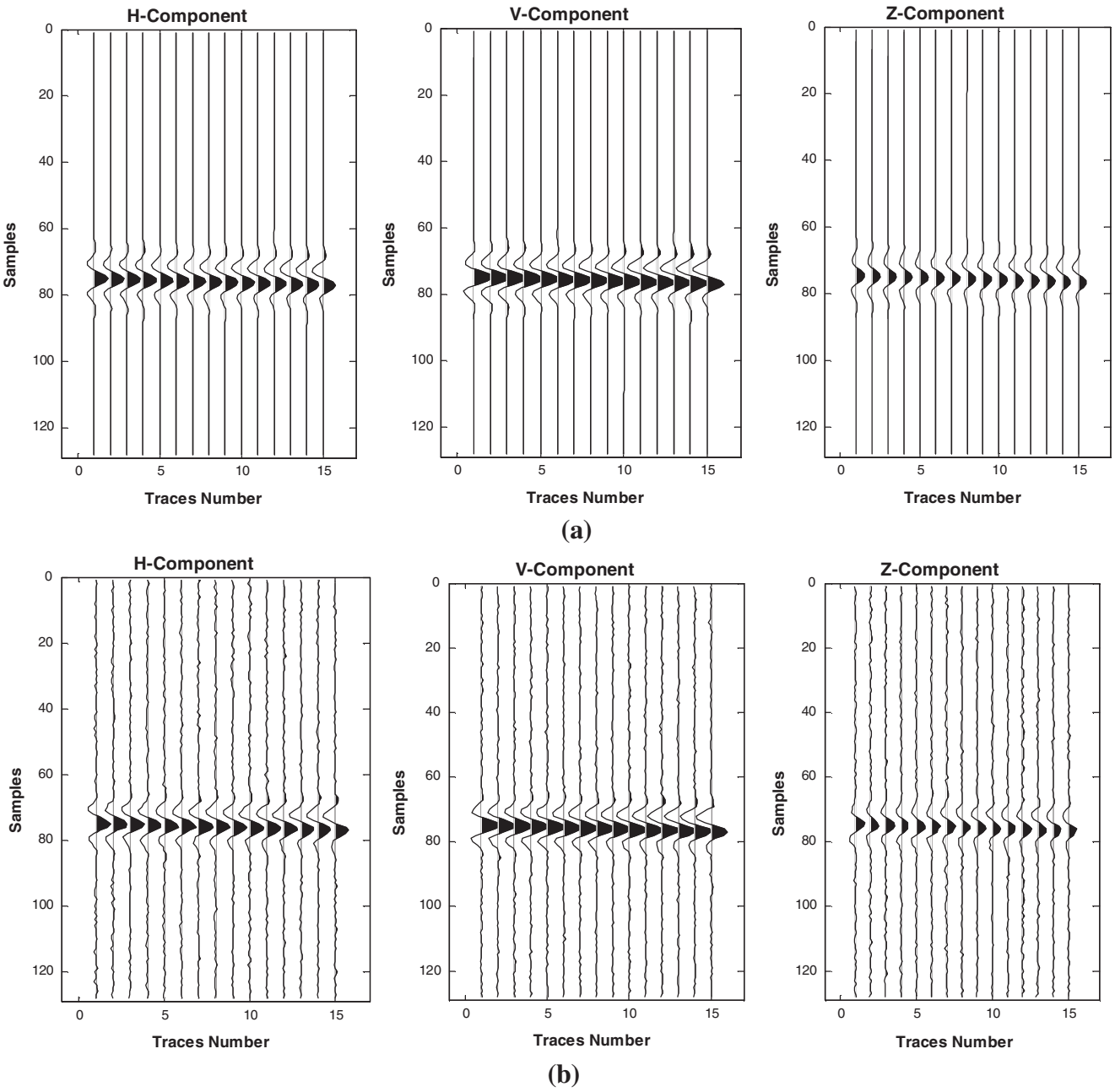

Figure 9 (a) Multicomponent seismic wavefield model for second wave. (b) Second separated seismic wave from noisy multicomponent seismic wavefield data set.

covariance matrix $\hat{\mathbf{E}}_{\mathbf{Xa},wave1}(f)$, $\hat{\mathbf{E}}_{\mathbf{Xa},wave2}(f)$. Therefore, projecting the vector $\mathbf{y}(f)$ onto only the first eigenvector $\mathbf{u}_1(f)$ will result in obtaining the first seismic wave. Similarly, by projecting $\mathbf{y}(f)$ onto only the second eigenvector $\mathbf{u}_2(f)$ will result in obtaining the second seismic wave as in Eqs. (19) and (20):

$$\mathbf{y}_{wave1}(f) = \langle \mathbf{y}(f), \mathbf{u}_1(f) \rangle \cdot \mathbf{u}_1(f) = \frac{\mathbf{u}_1(f)^H \mathbf{y}(f) \mathbf{u}_1(f)}{\|\mathbf{u}_1(f)\|_2^2} \tag{19}$$

$$\mathbf{y}_{wave2}(f) = \langle \mathbf{y}(f), \mathbf{u}_2(f) \rangle \cdot \mathbf{u}_2(f) = \frac{\mathbf{u}_2^H(f) \mathbf{y}(f) \mathbf{u}_2(f)}{\|\mathbf{u}_2(f)\|_2^2} \tag{20}$$

The last steps consist of rearranging long data vectors ($\mathbf{y}_{wave1}(f)$, $\mathbf{y}_{wave2}(f)$) of the first and the second seismic waves into a multicomponent form given in Eq. (2) and then taking the inverse Fourier transform on $\underset{\equiv wave1}{Y} \in \mathsf{E}^{K_d \times K_x \times K_f}$ and $\underset{\equiv wave2}{Y} \in \mathsf{E}^{K_d \times K_x \times K_f}$ respectively to map them to the time-domain.

4. Results and analysis

In this section, many experiments have been conducted on a noisy synthetic and real multi-component wave-field seismic data to examine the effectiveness of the proposed approach.

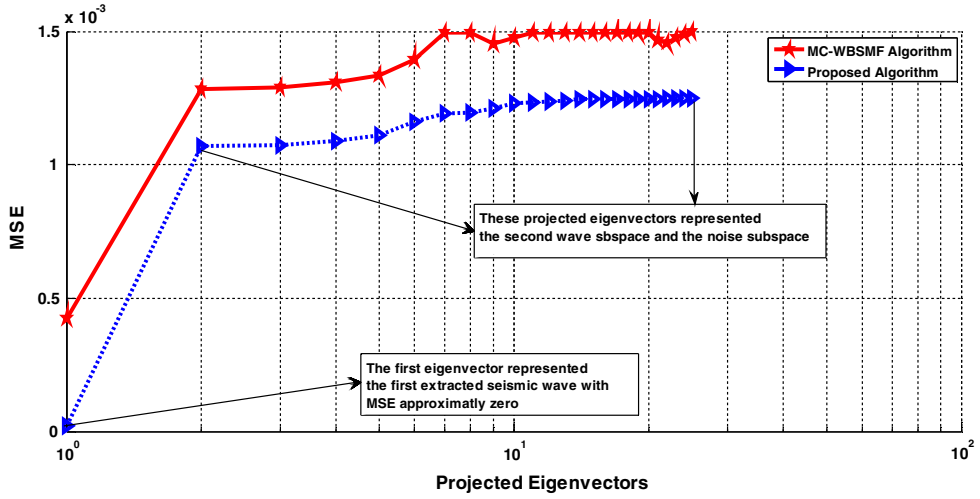

Figure 10 Evaluation of MSE versus projected eigenvector for the first separated seismic wave.

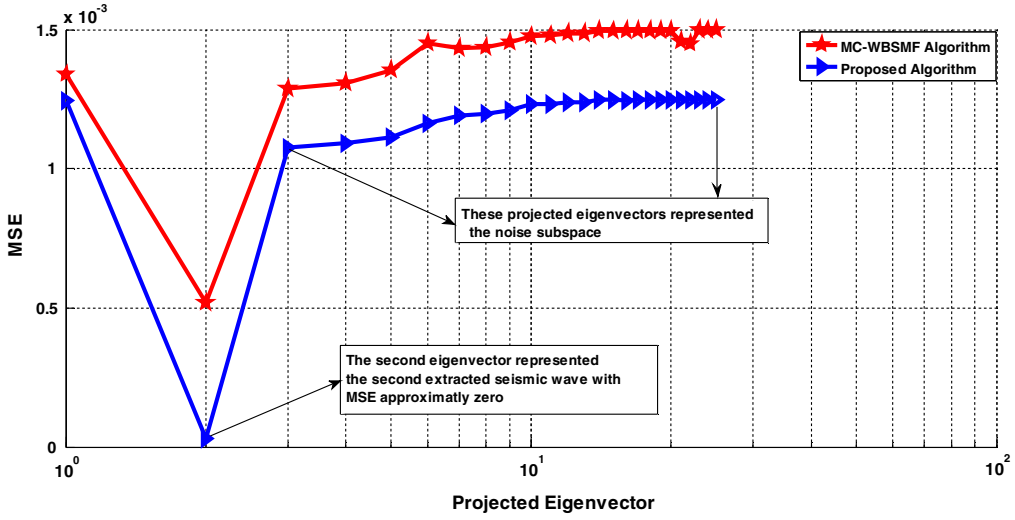

Figure 11 Evaluation of MSE versus projected eigenvector for the second separated seismic wave.

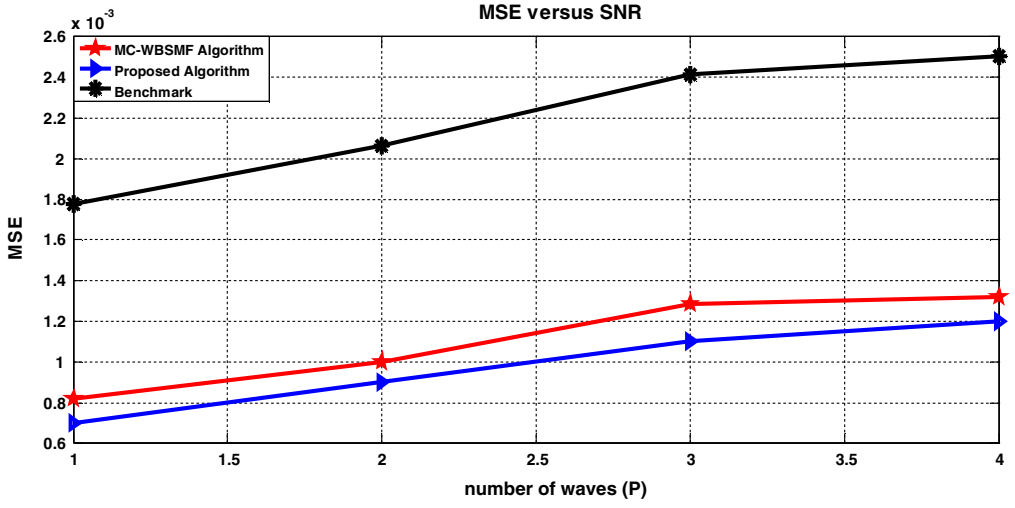

Figure 12 Evaluation of MSE versus the number of seismic waves for separation process.

4.1. Blind separation of seismic waves from synthetic noisy multicomponent seismic wavefield

In this section, the capability of the proposed algorithm to blindly separate different polarized seismic waves from the noisy multi-component seismic wavefield is demonstrated. The parameters of the simulations have been set up as follows: Firstly, the multicomponent linear array is composed of 15 sensors, each of which is made up of three components. The first component relates to the geophone H, the second component to the geophone V, and the third component to the geophone Z. Secondly, the recording time was set to 256 ms, which corresponds to 128 time samples. Finally, the spatial and frequency smoothing order is set to be equal to two therefore $(N_S = 2, N_f = 2)$ where $N = (2N_S + 1)(2N_f + 1)$ then we have $N = 25$. In this simulation, two seismic waves have been used, one has linear polarization and the other has an elliptical polarization. $(P = 2)$. Fig. 6 shows the noisy synthetic multicomponent seismic wavefield that is recorded on the H, V, Z components respectively. The white

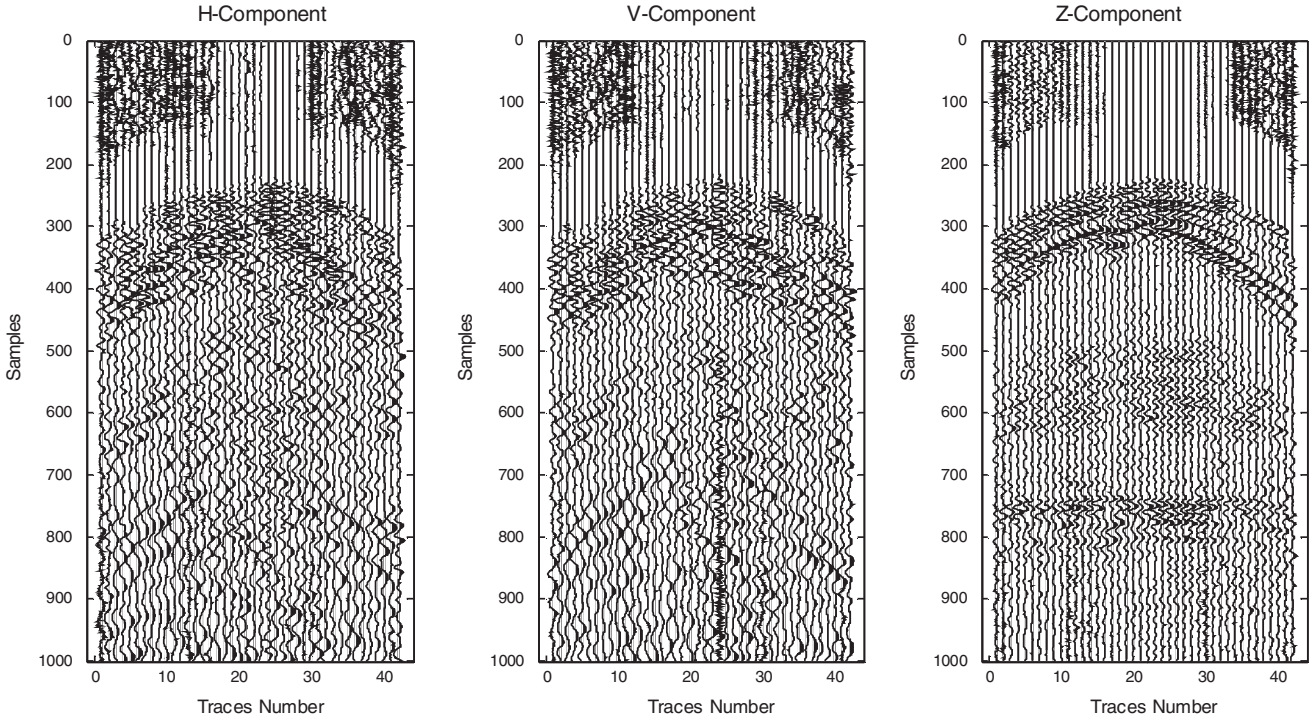

Figure 13 The initial real noisy multicomponent seismic wavefield.

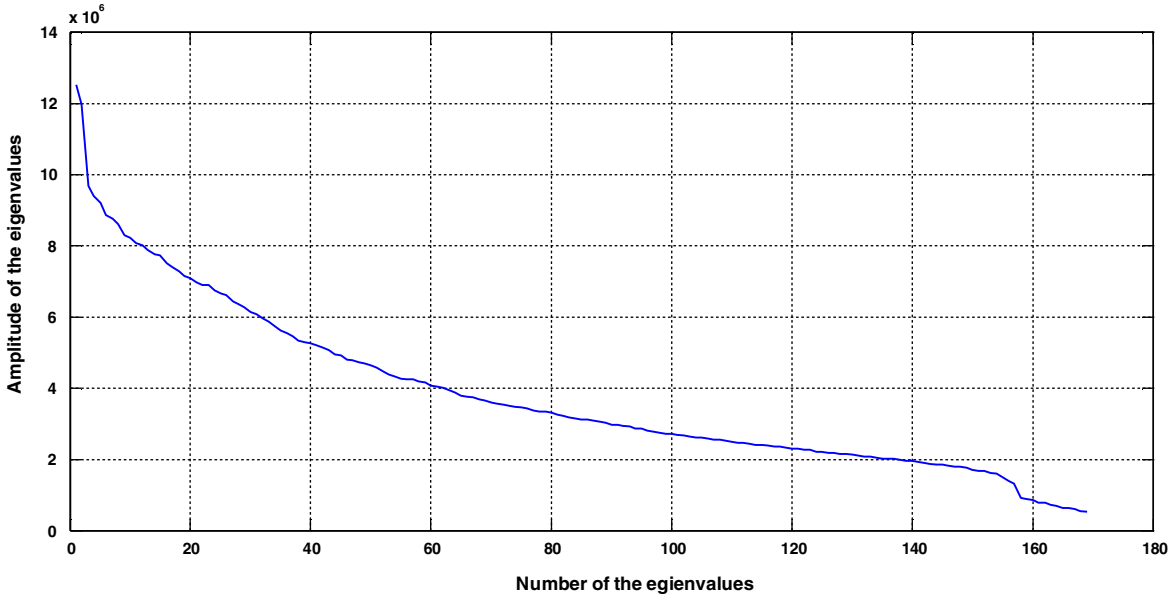

Figure 14 Eigenvalue amplitude of estimated reduced dimension covariance spectral matrix.

Gaussian noise is uncorrelated with the seismic waves and it is equally distributed for all components with SNR = 1.5 dB.

Fig. 7 shows the amplitude of twenty-five eigenvalues $\lambda_{i=1,2,\ldots,25}$ that relate to the reduced dimension eigenvector matrix $\mathbf{U}(f)$ in Eq. (17). Consequently, it is noticed that the first two eigenvalues have the highest amplitude where the first eigenvalue corresponds to the first seismic wave while the second eigenvalue corresponds to the second seismic wave.

The mathematical basis for the separation of these two waves has been presented in Eqs. (18)–(20). Fig. 8a shows the original seismic wave model that has linear polarization and Fig. 9a shows the original seismic wave model with elliptical polarization.

Moreover, Figs. 8b and 9b present the separated linear and elliptical waves respectively after applying the proposed blind separation algorithm. To gauge the performance of the proposed algorithm in terms of separating seismic waves over the MC-WBSMF algorithm, the MSE criteria between the separated seismic wave and modeled seismic wave are used:

$\mathrm{MSE} = \frac{1}{\mathrm{TP}}\sum_{t=1}^{\mathrm{T}}\sum_{i=1}^{\mathrm{P}}[\mathbf{x}_i(t) - \hat{\mathbf{x}}_i(t)]^2$, where $\mathbf{x}_i$ is defined as the ith modeled (original) seismic wave and $\hat{\mathbf{x}}_i$ is defined as the ith separated seismic wave. The MSE values in Fig. 10 for separating the first seismic wave are obtained by projecting the long data vector $\mathbf{y}(f)$ onto the 25 eigenvectors of $\mathbf{U}(f)$ matrix and comparing the resultant seismic data acquired from this projection step with the multicomponent seismic wavefield model in Fig. 8a. The exceptional observation to appear from Fig. 10 is that the lowest MSE value is obtained by projecting only the first eigenvector of reduced dimension spectral covariance matrix that has the highest eigenvalue onto the long data vector $\mathbf{y}(f)$. This indicates that the first eigenvector that is related to the highest eigenvalue represents the first seismic wave.

Similarly, it can be revealed from Fig. 11 that the lowest MSE value for separating the second seismic wave is found in the second eigenvector, this means that the second eigenvector that has the second highest eigenvalue related to the second seismic wave. It is important to point out that the x-axis in Figs. 10 and 11 relates to the eigenvectors of matrix $\mathbf{U}(f)$, such that when $x = 2$ it corresponds to the second eigenvector only. The proposed algorithm has been conducting four times on a noisy synthetic multicomponent seismic wavefield that contains a number of seismic waves varying from 1 to 4. The MSE values between the separated seismic wave and modeled seismic wave versus the number of seismic waves are shown in Fig. 12. The lowest MSE value is obtained when the seismic wavefield that contain only one seismic wave. The MSE values go up as the number of seismic waves in the wavefield increase. Indeed, the proposed algorithm has improved the MSE by average of 11.5% over the MC-WBSMF algorithm. Moreover, the benchmark that refers to the noisy seismic waves is used to

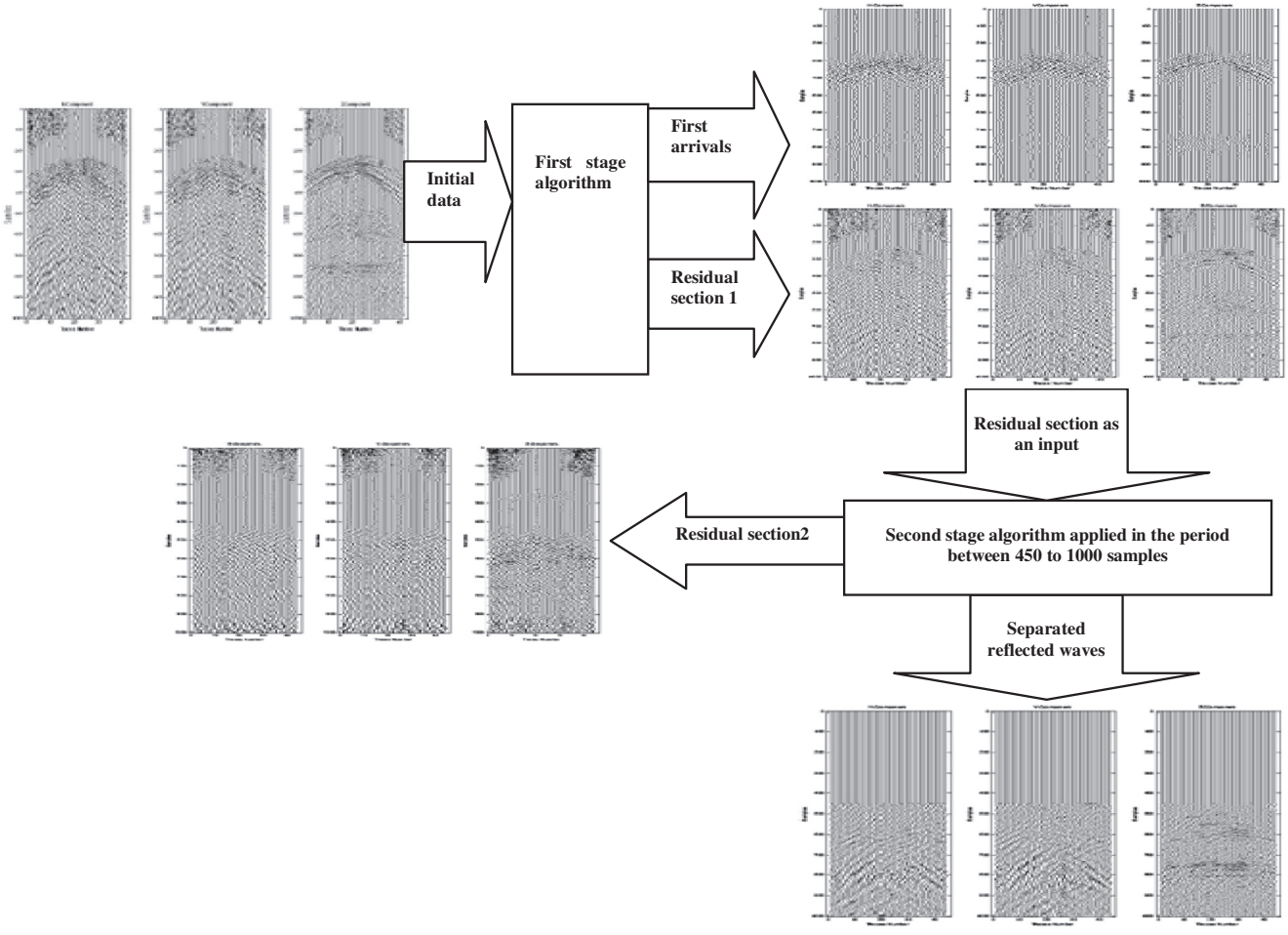

Figure 15 Block diagram of separation of both first arrivals and reflected waves.

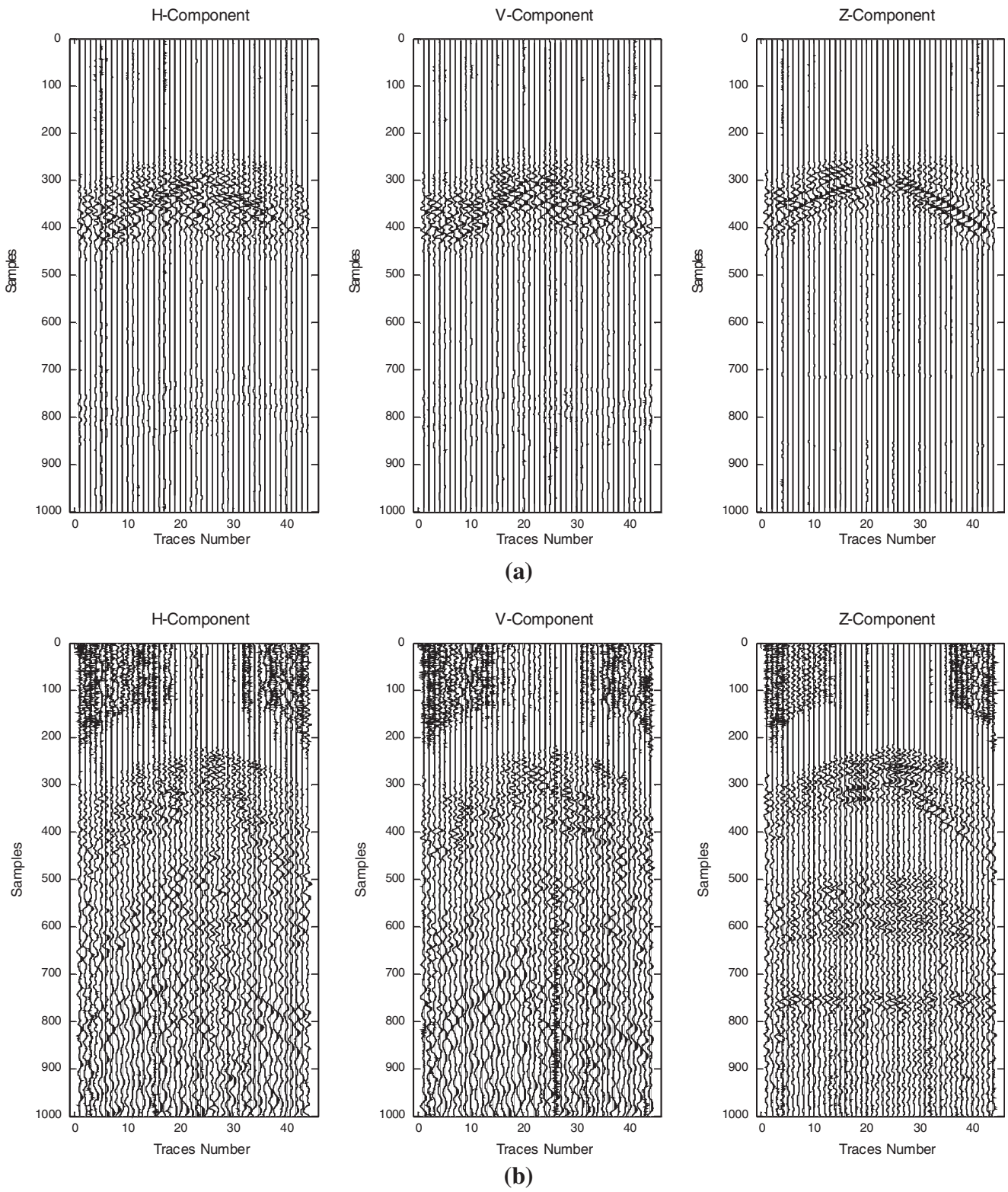

Figure 16 (a) Separated first arrival waves. (b) First section residual.

evaluate the effectiveness of the proposed algorithm in terms of separating seismic waves. Another significant outcome from Fig. 12 is that the MSE values of the proposed algorithm have been reduced by the average of 79% over the benchmark.

4.2. Blind separation of real seismic wavefield

In this section, the proposed algorithm is applied to real multicomponent seismic wavefield data to show the applicability

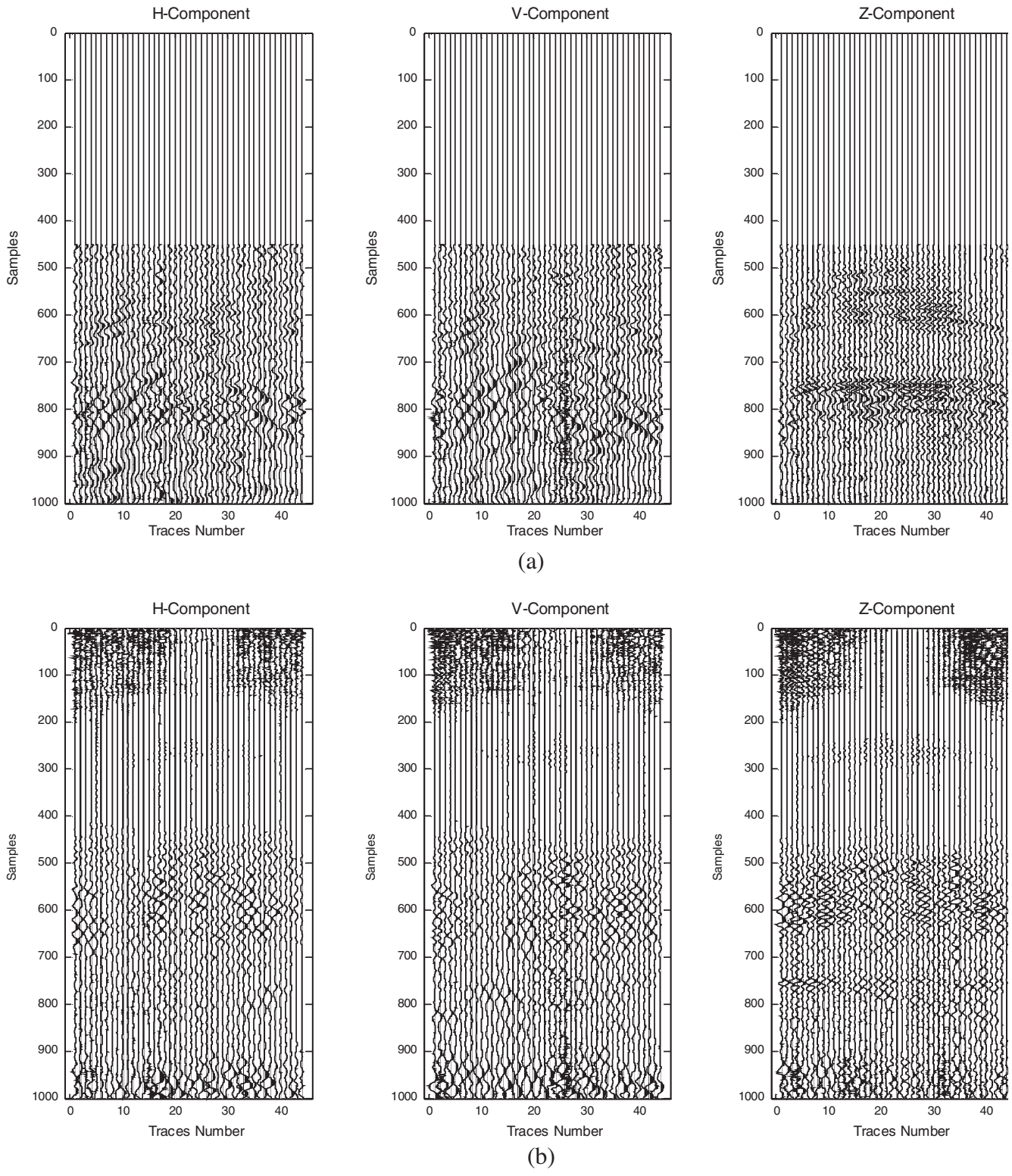

Figure 17 (a) Separated reflected waves. (b) Second section residual.

of the proposed method to blindly separate different seismic wavefields according to their energy. The real multicomponent seismic wavefield data set is obtained using dynamite sources and a linear array of three component geophones (3C-3D) in the Blackfoot area of Alberta, Canada (CREWES, 2013). According to Fig. 13, the initial real seismic data composed of 42 sensors each of which is made of three components. Every sensor comprises three vector geophones which are

recording the underground motion displacement in three orthogonal directions noted as H, V, Z. It can be shown from Fig. 13 that the direct arrivals as well as the refracted waves' energy are recorded during the sample period 270–450. In addition, the reflected waves embedded with noise lay in the period of 500–950 samples. From a visual inspection, the SNR is relatively poor, especially for horizontal components (H and V). The distance between adjacent geophones is 60 m.

The data sampling rate is set to 2 ms/sample, the recording time is 2 s, which corresponds to $K_t = 1000$ samples. In this experiment, the spatial and frequency smoothing order have been set to be equal to six, i.e. $N_S = 6$, $N_f = 6$, so that $N = (2N_S + 1)(2N_f + 1)$ gives $N = 169$. As a result the dimension of derived reduced spectral covariance matrix will be (169×169). Fig. 14 depicts the amplitude of one hundred sixty-nine eigenvalues of the reduced dimension covariance spectral matrix $\lambda_{i=1,2,\ldots,169}$ that are related to the eigenvector matrix $\mathbf{U}(f)$ in Eq. (17). Taking into account all above parameters that have been set, two sets of experiments have been conducted on real multicomponent seismic wavefield.

The experiment aims to blindly separate both first arrivals as well as the reflected waves. This can be accomplished by applying the proposed algorithm in two stages as shown in Fig. 15. In the first stage of processing, given only the real noisy multicomponent seismic wavefield as an input to the proposed algorithm, the first arrival waves that have the highest energy have been blindly separated.

Fig. 16a presents the separated first arrival waves (i.e. the refracted energy and the direct arrivals) by projecting the first ten eigenvectors of matrix $\mathbf{U}(f)$ that have the highest eigenvalues onto the long data vector $\mathbf{y}(f)$. The first arrival waves are used to determine the velocity and thickness of the near surface layer which is necessary to calculate static correction. Basically, the reflected waves are used to obtain an image of the earth subsurface lithography. While these waves have a low energy, the first stage processing was used to remove the waves with the highest energy (i.e. first arrivals waves). The difference between initial real data set and separated first arrival waves, given in Fig. 16b, is subsequently used as an input to the second stage of processing.

Fig. 17a shows the blindly separated reflected waves which result from conducting the second stage processing on first residual section in the period of 500–950 samples. The second residual section in Fig. 17b contains the noise extracted from the reflected waves. The second experiment aims to show the ability of the proposed algorithm to enhance the SNR of the noisy real seismic wavefield.

5. Conclusion

The purpose of this paper was to develop a less complex blind separation algorithm for noisy multicomponent seismic wavefields. The strength of the proposed work lies in a number of sub areas as follows:

- The noisy multicomponent seismic wavefield in the form of frequency transformed matrix model has been derived and used as a framework for developing the proposed algorithm.
- During the mathematical analysis of the proposed algorithm in Section 3, a significant reduction in the spectral covariance matrix dimensions has been mathematically achieved. Therefore, the eigenvector matrix $\mathbf{U}(f)$ of the spectral covariance matrix $\hat{\mathbf{E}}_{\mathbf{yy}1}(f)$ has been derived by means of the eigenvector matrix $\mathbf{V}(f)$ of reduced dimension spectral covariance matrix $\hat{\mathbf{E}}_{\mathbf{yy}2}(f)$. This leads to a significant decrease in computational operations.
- The proposed algorithm has the ability to blindly separate different seismic wavefields, according to their energy, from real noisy multicomponent seismic wavefields.
- We have used the MSE criteria to evaluate the performance of the proposed algorithm. The proposed novel algorithm has shown a marked improvement by 11.5% in terms of separating seismic waves over the MC-WBSMF algorithm.

References

Al-anboori, A., van der Baan, M., Kendall, J.M., 2005. Approximate separation of pure mode and converted waves in 3-C reflection seismic by τ–p transform. Geophysics 70 (3), 81–86.

Al-Qaisi, A.W.S., Woo, W.L., Dlay, S.S., 2008. Novel statistical approach to blind recovery of earth signal and source wavelet using independent component analysis. Wseas Trans. Signal Process. 4 (4), 231–240.

Benoliel, S.D., Schneider, W.A., Shurtleff, R.N., 2006. Frequency wavenumber approach of the τ–p transform: some applications in seismic data processing. Geophysics 35 (5), 517–538.

CREWES (Consortium for Research in Elastic Wave Exploration Seismology), 2013. <www.crewes.org>.

Embree, P., Burg, J.P., Backus, M.M., 1963. Wide band velocity filtering—the pie-slice process. Geophysics 28 (6), 948–974.

Foster, D.J., Mosher, C.C., 1992. Suppression of multiple reflections using the radon transform. Geophysics 57 (3), 386–395.

Hanna, M., 1988. Velocity filters for multiple interference attenuation in geophysical array data. IEEE Trans. Geosci. Remote Sens. 26 (6), 741–748.

Natasha Hendrick. Multi-component seismic wavefield separation via spectral matrix filtering. ASEG2006 extended abstract-18th Geophysical conference. Melbourne, Australia, 2006.

Kirlin, R., 2001. Data covariance matrices in seismic signal processing. Can SEGRec 26 (4), 18–24.

Le Bihan, N., Mars, J.I., 2004. Singular value decomposition of quaternion matrices: a new tool for vector-sensor signal processing. Signal Process. 84 (7), 1177–1199.

Ling, G., Ren, S.X., 2013. A blind source separation method applied to simultaneous kinetic multicomponent determination. Appl. Mech. Materials 380–384, 3678–3681.

Liu, B.T., 2014. Covariance-based wavefield separation and its application in crosswell seismic data. Appl. Mech. Materials 519–520, 1025–1029.

Mari, J.L., Glangeaud, F., 1990. Spectral matrix filtering applied to VSP processing. Revuede l'Institut Français du Pétrole 45 (3), 417–434.

Paulus, Caroline, Mars, Jerome I., 2006. New multicomponent filters for geophysical data processing. IEEE Trans. Geosci. Remote Sens. 44 (8), 2260–2270.

Paulus, C., Gounon, P., Mars, J.I., 2005. Wideband spectral matrix filtering for multicomponent sensor array. Signal Process. 85 (9), 1723–1743.

Pillai, S.U., Kwon, B.H., 1989. Forward backward spatial smoothing techniques for coherent signal identification. IEEE Trans. Acoust. Speech Signal Process. 37 (1), 8–15.

Rao, B.D., Hari, K.V.S., 1993. Weighted subspace methods and spatial smoothing: analysis and comparison. IEEE Trans. Signal Process. 41 (2), 788–803.

Rutty, M.J., Jackson, G.M., 1992. Wavefield decomposition using spectral matrix techniques. Explor. Geophys. 23 (2), 293–298.

Vrabie, V.D., Mars, J.I., Lacoume, J.-L., 2004. Modified singular value decomposition by means of independent component analysis. Signal Process. 84 (3), 645–652.

Zhou, Binzhong, Greenhalgh, Stewart, 2006. Multiple suppression by 2D filtering in the parabolic τ–p domain: a wave-equation-based method. Geophysics 44 (3), 375–401.